The Small Molecule Dispergo Tubulates the Endoplasmic Reticulum and Inhibits Export

The small molecule dispergo tubulates the endoplasmic reticulum and inhibits export

Lei Lu[a,b,*], Rami N. Hannoush[a,c,d,*], Brian C. Goess[c,e], Shankar Varadarajan[f], Matthew D. Shair[c], and Tom Kirchhausen[a]

[a]Department of Cell Biology, Harvard Medical School, and Program in Cellular and Molecular Medicine at Children's Hospital, Boston, MA 02115; [b]School of Biological Sciences, Nanyang Technological University, Singapore 637551; [c]Department of Chemistry and Chemical Biology, Harvard University, Cambridge, MA 02138; [d]Department of Early Discovery Biochemistry, Genentech, South San Francisco, CA 94080; [e]Department of Chemistry, Furman University, Greenville, SC 29613; [f]MRC Toxicology Unit, University of Leicester, Leicester LE1 9HN, United Kingdom

ABSTRACT **The mammalian endoplasmic reticulum (ER) is an organelle that maintains a complex, compartmentalized organization of interconnected cisternae and tubules while supporting a continuous flow of newly synthesized proteins and lipids to the Golgi apparatus. Using a phenotypic screen, we identify a small molecule, dispergo, that induces reversible loss of the ER cisternae and extensive ER tubulation, including formation of ER patches comprising densely packed tubules. Dispergo also prevents export from the ER to the Golgi apparatus, and this traffic block results in breakdown of the Golgi apparatus, primarily due to maintenance of the constitutive retrograde transport of its components to the ER. The effects of dispergo are reversible, since its removal allows recovery of the ER cisternae at the expense of the densely packed tubular ER patches. This recovery occurs together with reactivation of ER-to-Golgi traffic and regeneration of a functional Golgi with correct morphology. Because dispergo is the first small molecule that reversibly tubulates the ER and inhibits its export function, it will be useful in studying these complex processes.**

Monitoring Editor
Benjamin S. Glick
University of Chicago

Received: Aug 6, 2012
Revised: Jan 23, 2013
Accepted: Jan 30, 2013

INTRODUCTION

The mammalian endoplasmic reticulum (ER) is a large membrane network of interconnected cisternae or sheets and tubules located throughout the cytosol (Baumann and Walz, 2001; Shibata *et al.*, 2006; Lu *et al.*, 2009, 2011). Protein and lipid synthesis and certain posttranslational modifications occur within its membrane-bound compartments. During mitosis, the ER architecture undergoes a major rearrangement to extended cisternae, with a very small fraction remaining organized as tubules (Lu *et al.*, 2009, 2011). During interphase newly made secretory proteins leave the ER in COPII-based transport carriers, which bud from specialized ER exit sites (ERES) scattered throughout the ER. These carriers coalesce to form the vesicular-tubular network of the so-called ER Golgi intermediate compartment (ERGIC). Elements of the intermediate compartment that contain newly synthesized proteins are continuously transported along microtubules toward the perinuclear region, where they deliver their contents to the *cis* face of the Golgi apparatus. Fully processed proteins exit at the opposite end of the Golgi, the *trans* face, to reach the *trans*-Golgi network (TGN), from which they are transported to the plasma membrane and endosomes (Emr *et al.*, 2009).

The dynamics of the Golgi apparatus, critical for all its functions, can be studied by the use of reagents that trap the Golgi in states that are usually sparsely populated or are not present in a normal cell. Cell-permeable small molecules with these properties are useful, particularly because they can be specific, fast acting, and reversible, allowing detailed study of Golgi disassembly and reassembly. In contrast, no equivalent chemicals are available to study the organization and function of the ER. By use of a phenotypic screen of inhibitors of exocytic vesicular traffic, we discovered a small molecule, which we call dispergo ("disrupt ER and Golgi"),

This article was published online ahead of print in MBoC in Press (http://www.molbiolcell.org/cgi/doi/10.1091/mbc.E12-08-0575) on February 6, 2013.

*These authors contributed equally.

Address correspondence to: Tom Kirchhausen (Kirchhausen@crystal.harvard.edu)

Abbreviations used: CCD, charge-coupled device; DMSO, dimethyl sulfoxide; DTT, dithiothreitol; ERES, ER exit site; ERGIC, ER Golgi intermediate compartment; FRAP, fluorescence recovery after photobleaching; GalT, β-glactosyltransferase; NRK, normal rat kidney; VSVGts, temperature-sensitive mutant vesicular stomatitis virus glycoprotein G.

that causes a rapid change in the architecture of the ER, involving loss of cisternae and extensive tubulation, including formation of densely packed tubules throughout the cytoplasm, rendering export from the ER nonfunctional. Lack of anterograde transport from the ER eventually causes loss of the Golgi apparatus together with retention of its contents in the ER. Removal of dispergo leads to reestablishment of the ER architecture: ER cisternae reappear, densely packed ER tubules disappear, membrane transport from the ER reactivates, and a functional Golgi apparatus reassembles.

RESULTS

Identification of dispergo as an inhibitor of VSVG^{ts}–green fluorescent protein export from the ER

Using an image-based, high-throughput phenotypic assay that we developed previously for inhibitors of VSVG^{ts}–green fluorescent protein (GFP) exocytic vesicular traffic (Feng *et al.*, 2003) to screen a diversity-oriented library of 10,000 small molecules resembling the natural product carpanone, we identified a number of compounds that block VSVG^{ts}-GFP exit from the Golgi or cause Golgi fragmentation (Goess *et al.*, 2006). We chose to use a natural product as the core structure for the diversity-oriented synthesis because we hypothesized that such structures would have a higher intrinsic ability to bind proteins. This strategy proved to be successful, as shown by our recent discovery of secramine, a cell-permeable, galanthamine-like molecule found to be an inhibitor of vesicular traffic from the Golgi by interference with the function of the small GTPase Cdc42 (Pelish *et al.*, 2006). We describe here a new molecule identified in the same screen, which we call dispergo (Figure 1A). It inhibits, with $IC_{50} \approx 6.8$ μM, traffic of VSVG^{ts}-GFP from the ER to the plasma membrane in BSC1 cells upon transfer from 40 to 32°C (Figure 1, B and C); it is also active in HeLa and Chinese hamster ovary cells (unpublished data). Carpanone (Figure 1A), which inspired the library from which dispergo was identified, is inactive (Figure 1, B and C); in its presence, as in untreated cells, VSVG^{ts}-GFP accumulates in the ER in cells kept at 40°C and rapidly reaches the Golgi apparatus and the plasma membrane soon after transfer to 32°C.

In addition to rapidly inhibiting VSVG^{ts}-GFP traffic to the plasma membrane, dispergo also prevented VSVG^{ts}-GFP from reaching the Golgi apparatus marked with GalT-tomato (compare the control in Figure 2A with dispergo in Figure 2, B and C). Instead we saw the appearance of bright VSVG^{ts}-GFP patches in cells maintained at 40°C or in cells transferred from 40 to 32°C (Figure 2, B and D); these VSVG^{ts}-GFP patches colocalized with newly formed patches of the ER marker TRAPα (Figure 2D).

Reversible changes of the ER architecture induced by dispergo

We then followed the effect of dispergo on the distribution of another ER marker, GFP- Sec61β, and found the rapid accumulation of bright GFP-Sec61β patches (Figure 3A, top, arrowheads, and Supplemental Movie S2). The appearance of the ER patches coincided with extensive ER tubulation and loss of ER cisternae (Figure 3B, solid arrowheads). The effect of dispergo on the ER architecture was reversible, as demonstrated by the disappearance of the ER patches during the washout period along with the abrupt reappearance of ER cisternae (Figure 3C); eventually, the cells recovered the characteristic combination of cisternae and tubules in interphase cells. GFP-Sec61β within the dispergo-induced patches exchanged rapidly, presumably though direct connections between the patches and the surrounding ER, as shown by the relatively fast recovery of fluorescence signal in photobleached patches, with half-times in the range of 20–100 s (Figure 3, D and E, and Supplemental Movie S3).

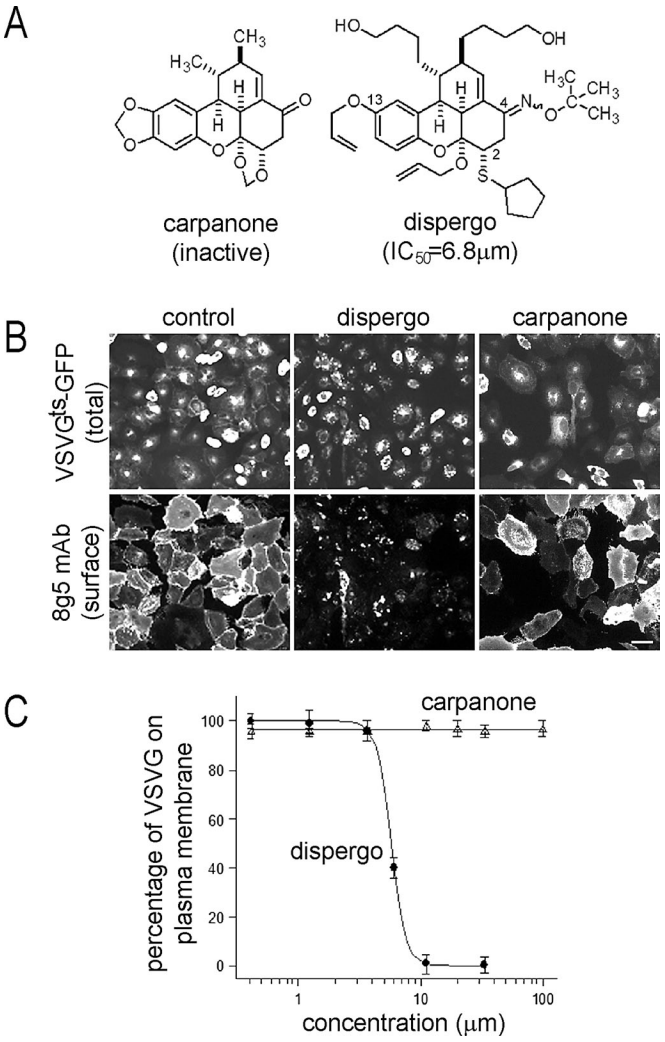

FIGURE 1: Dispergo inhibits the traffic of VSVG^{ts}-GFP from the ER to the plasma membrane. (A) Structures of synthetic dispergo and the related natural product carpanone. (B) Inhibitory effect of dispergo on the arrival of VSVG^{ts}-GFP to the cell surface. BSC1 cells were transduced with adenovirus to express VSVG^{ts}-GFP overnight at 40°C. Cells were subsequently incubated with DMSO (control), dispergo, or carpanone at the nonpermissive temperature (40°C) for 1 h, followed by incubation at the permissive temperature (32°C) for 3 h. VSVG^{ts} at the cell surface was detected by incubation by the 8G5 monoclonal antibody specific for the ectodomain of VSVG. Scale bar, 60 μm. (C) The effect of dispergo on the arrival of VSVG^{ts}-GFP to the cell surface was quantified by determining for each cell the ratio of the surface 8G5 fluorescence signal corrected by background to the total VSVG^{ts}-GFP fluorescence signal. Data are presented as a semilog plot for results obtained from ~1500 cells imaged in three independent experiments. Values for each point are mean ± SD; the IC_{50} (~6.8 μM) was calculated as the concentration at which 50% of the VSVG signal was present at the cell surface.

The effect of dispergo on the organization of the ER also occurred in cells whose protein synthesis was acutely blocked by cycloheximide treatment (unpublished data).

These observations led us to examine in more detail the effects of dispergo on the architecture of the ER. Thin-section transmission electron microscopy of cells treated with dispergo indicate the appearance of numerous clusters containing densely packed membrane profiles ~50 nm in diameter (Figure 3F, solid arrowheads)

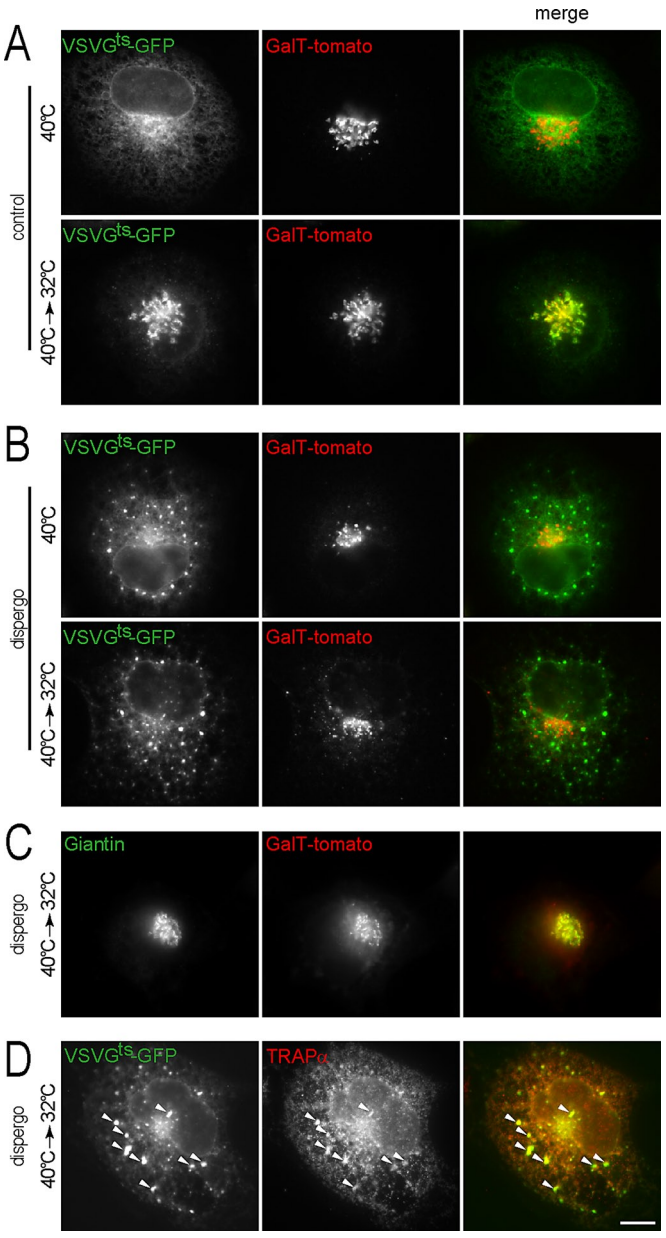

FIGURE 2: Dispergo inhibits the traffic of VSVG^{ts}-GFP from the ER to the Golgi apparatus. BSC1 cells stably expressing GalT-tomato were transduced with adenovirus to express VSVG^{ts}-GFP overnight at 40°C. Cells were then treated with DMSO (control) or dispergo for 40 min at 40°C and subsequently shifted to 32°C for 20 min. (A) Control cells treated with DMSO only. (B–D) Cells treated with dispergo. Note in B the redistribution of VSVG^{ts}-GFP into patches in cells kept at 40°C during the dispergo treatment. (C) Under these experimental conditions, a significant amount of GalT-tomato colocalized with Giantin, validating the use of GalT-tomato as a Golgi marker. Endogenous Giantin was identified by immunostaining. (D) Colocalization of VSVG^{ts}-GFP patches with endogenous TRAPα, an ER marker (arrowheads) visualized by immunostaining in cells treated with dispergo. All images were from fixed BSC1 cells acquired using wide-field fluorescence microscopy. Scale bar, 10 μm.

interpreted as cross sections of tubular structures (Figure 3F, enlargement) and absence of stacked ER membranes. The cytosolic surface of these membrane profiles were smooth, and the clusters were often associated with additional membrane profiles, ~100 nm wide, extending toward adjacent regions within the cytosol, perhaps communicating with other clusters or with the rest of the ER (Figure 3F, enlargement, open arrowheads). We found no morphological evidence to support the presence of a limiting membrane surrounding the tubular clusters.

The patches induced by dispergo contained the ER membrane marker HA-DP1 (Supplemental Figure S1A), the endogenous ER luminal protein calreticulin (Supplemental Figure S1B), and the ER retention signal KDEL fused to GFP (ss-GFP-KDEL; Supplemental Figure S1C). The fluorescence intensities associated with calreticulin or ss-GFP-KDEL in the ER patches were significantly lower (Supplemental Figure S1, B and C, arrowheads), consistent with a lower volume-to-membrane ratio in tubules than in cisternae. Similar ER patches tracked with these markers were also observed in other cells, such as NRK, HeLa, Ptk2, and mouse MEF cells (unpublished data). We note that dispergo treatment led to efficient formation of ER patches in cells that did not express ER protein markers (Supplemental Figure S1, D, E, and F), suggesting that the patches do not correspond to the organized smooth ER associated with the stacking of smooth ER (Snapp *et al.*, 2003) or to patches of smooth ER induced by phenyl-2-decanoyl-amino-3-morpholino-1-propanol-hydrochloride (Sprocati *et al.*, 2006), as these ER morphologies only seem to appear upon ectopic overexpression of ER membrane proteins.

Generation and maintenance of the ER tubular network require the presence of microtubules (Terasaki *et al.*, 1986; Waterman-Storer and Salmon, 1998; Lu *et al.*, 2009). We found, however, that the extensive ER tubulation induced by dispergo treatment does not depend on the microtubule network. We first treated BSC1 cells with nocodazole to depolymerize microtubules, leading to loss of ER tubules and formation of ER cisternae (Figure 3G, left; Lu *et al.*, 2009). We then followed this treatment by incubating with nocodazole and dispergo together for 3 h and found that dispergo induced formation of ER tubules and ER patches at the expense of ER cisternae, despite the continued presence of an inhibitor of microtubule dynamics (Figure 3G, right).

Dispergo disrupts recruitment of exocytic cargo to the ERES

Cargo export from the ER to the Golgi apparatus is mediated by vesicular carriers that form at ERES and contain Sec31a, a component of the COPII coat (Lee *et al.*, 2004). Because dispergo inhibits the ER export of VSVG^{ts}-GFP (Figure 2B), we asked whether dispergo might inhibit ER export by preventing the recruitment of Sec31a to ERES. We found no statistical difference ($p = 0.40$) in the density of Sec31a-containing fluorescent spots in the absence (0.25 ± 0.05 μm^{-2}; $n = 20$ cells) or presence of dispergo (0.21 ± 0.07 μm^{-2}; $n = 15$ cells; Supplemental Figure S2A). In contrast to these results, we found that VSVG^{ts}-GFP failed to accumulate at ERES in cells treated with dispergo. In control cells not treated with dispergo and maintained at the nonpermissive temperature of 40°C, VSVG^{ts}-GFP displayed the expected homogeneous distribution throughout the ER and absence of concentration in the ERES marked with Sec31a (Figure 4A). A 10-min incubation at the permissive temperature of 32°C led to the expected concentration of VSVG^{ts}-GFP on the ERES and its accumulation in the perinuclear region associated with the Golgi apparatus (Figure 4B). In contrast, cells treated with dispergo at 40°C accumulated VSVG^{ts}-GFP in patches, which did not colocalize with Sec31a in ERES (Figure 4C). Transfer of the dispergo-treated cells from 40 to 32°C confirmed both loss of VSVG^{ts}-GFP export from the ER and accumulation of VSVG^{ts}-GFP as patches that did not colocalize with Sec31a at ERES (Figure 4D). The same results were obtained

with cells kept at the permissive temperature for significantly longer times (unpublished data). We also determined the exchange dynamics between cytosolic and membrane bound COPII at the ERES using fluorescence recovery after photobleaching (FRAP) analysis and found that the exchange dynamics slightly increased upon dispergo treatment (Supplemental Figure S2). This result is in agreement with earlier observations demonstrating increased dynamic recruitment of COPII to ERES sites in the absence of cargo recruitment and vesicle budding (Forster *et al.*, 2006). These observations suggest that dispergo prevents access to ERES mainly by retaining VSVG^{ts}-GFP on ER patches.

Dispergo induces retention of Golgi proteins in the ER and consumption of the Golgi apparatus

Constituents of the Golgi apparatus continuously cycle between the Golgi and the ER (Storrie, 2005). The observed inhibition by dispergo of anterograde VSVG^{ts}-GFP traffic from the ER to the Golgi (Figures 1 and 2) led us to test whether dispergo also prevents ER export of Golgi components that cycle between the ER and the Golgi and to ask whether this inhibition would result in loss of the Golgi apparatus.

We examined the effects of dispergo on the localization of Golgi markers with known steady-state localizations. The following proteins marked the *cis*-Golgi: GPP130 (Linstedt *et al.*, 1997), GFP-ERGIC53 (Schindler *et al.*, 1993), KDEL receptor (Tang *et al.*, 1993), GM130 (Nakamura *et al.*, 1995), and β-COP (Oprins *et al.*, 1993); Giantin marked the medial Golgi (Linstedt *et al.*, 1995), and GalT-tomato marked the *trans*-Golgi. We also explored the effects of dispergo in the *trans*-Golgi network (TGN), as represented by Vti1a (Kreykenbohm *et al.*, 2002), TGN38 (Luzio *et al.*, 1990), Vamp4-GFP (Steegmaier *et al.*, 1999), and Golgin97 (Lu *et al.*, 2004). Dispergo treatment led to retention in the ER of all Golgi markers, except for Golgin97. The transmembrane proteins Vamp4-GFP (Figure 5A, arrowheads), GFP-ERGIC53 (Figure 5B, open arrowheads), KDEL receptor (Supplemental Figure S3A), and GalT-tomato (Figure 6A) also accumulated in the ER patches, whereas the transmembrane proteins GPP130 (Figure 5C), Giantin (Supplemental Figure S3B), Vti1a (Supplemental Figure S3C), and TGN38 (Supplemental Figure S3D) did not. The peripheral membrane protein Golgin97 (Supplemental Fig 3E) was released from the Golgi and appeared in the cytosol, whereas GM130 (Figure 5B) concentrated at the ERGIC in the vicinity of ERES labeled here with Sec31a (Figure 5B, arrowheads). Using GM130 as an "adopted ERES marker" in dispergo-treated cells, we found that β-COP relocalized to this region (Supplemental Figure S3F). In contrast to the accumulation of VSVG^{ts}-GFP in ER patches (Figure 2, B and D), the transmembrane protein GFP-ERGIC53 (Figure 5B) concentrated at the ERES and in the ER patches. We also found that rate of redistribution from the Golgi to the ER could vary significantly, as exemplified by the significant relocation of GM130 from the perinuclear Golgi region to the ERES in cells treated with dispergo for 20 min, whereas most of VAMP4-GFP remained in the perinuclear TGN (Figure 5D) in NRK cells.

To document the temporal relationship between the retention of Golgi components in the ER and the disappearance of the Golgi apparatus mediated by dispergo, we used spinning disk confocal microscopy to acquire time-lapse series from BSC1 cells coexpressing GFP-Sec61β and GalT-tomato (Figure 6A and Supplemental Movie S4). The first detectable ER patches, which contained the ER marker GFP-Sec61β but not the Golgi marker GalT-tomato, appeared <50 min after addition of dispergo; by this time, the drug had already blocked ER export of VSVG^{ts}-GFP (see Figures 2, B and D, and 4). After further dispergo treatment, the perinuclear fluorescence signal of GalT-tomato, which marks the Golgi apparatus, became barely detectable. Quantification of these observations is shown in Figure 6B. The temporal dissociation between appearance of ER patches (marked with GFP-Sec61β) and loss of the perinuclear Golgi signal (marked with GalT-tomato) suggests that loss of the Golgi apparatus is a secondary effect due to inhibition of ER export by dispergo.

The effects of dispergo are specific to the ER

In contrast to effects of dispergo on ER tubulation and the block in ER export, we were unable to detect perturbations in the clathrin-mediated uptake of fluorescently labeled transferrin (Supplemental Figure S4A). The dynamics of clathrin-dependent, endocytic coated-pit formation could be monitored as accumulation of the AP2 adaptor, on which dispergo had no effect (Supplemental Figure S4B, kymographs). Dispergo also had no effect on the distributions of early (Supplemental Figure S4C) and late endosomes/lysosomes (Supplemental Figure S4D), nor did it influence the organization of the actin and tubulin cytoskeleton (Supplemental Figure S4E and F). Close interactions between tubular ER and mitochondria have been described (de Brito and Scorrano, 2010; Friedman *et al.*, 2011); consistent with these observations, major alterations in the tubular ER organization led to mitochondrial fragmentation, as detected by MitoTracker staining in cells treated with dispergo (Supplemental Figure S4G).

ER stress does not induce formation of ER patches

To test whether cells subjected to ER stress might alter the ER morphology in a way similar to that observed upon dispergo treatment, we incubated BSC1 cells for 24 h with tunicamycin or dithiothreitol (DTT) and monitored the distribution of GFP-Sec61β and calreticulin. As illustrated by the results shown in the images in Supplemental Figure S5, generation of an acute ER stress response by treatment with these compounds did not generate ER patches and did not change in a detectable way the overall morphology of the ER.

DISCUSSION

In this study, we characterize the unique effects of the small molecule dispergo on the architecture of the ER and the associated strong inhibition of ER export. A secondary effect of dispergo is consumption of the Golgi apparatus, primarily due to loss of traffic in the anterograde but not the retrograde direction between the ER and the Golgi apparatus. The morphological effects of dispergo on the organization of the ER are unrelated to the perturbations generated during acute ER stress response or to the ER patches observed upon conditions of chemical perturbation with phenyl-2-decanoyl-amino-3-morpholino-1-propanolhydrochloride and organized smooth ER generated by ectopic overexpression of ER membrane proteins (Snapp *et al.*, 2003; Sprocati *et al.*, 2006). These effects are reversible and do not appear to affect endocytosis, the organization of the endosomal and lysosomal compartments, or the actin and microtubule cytoskeletons. A recent study, independently conducted by one of us, uncovered similar effects on the organization and function of the ER in cells treated with apogossypol (Varadarajan *et al.*, 2012).

The relatively fast onset of the perturbations induced by dispergo (17 ± 3 min; Figure 6B) suggests that it does not involve de novo synthesis of proteins, a conclusion we confirmed by observing the same effects of dispergo in cells whose protein synthesis was prevented by simultaneous treatment with cycloheximide (unpublished data).

We do not yet know how dispergo drives the transformation of ER cisternae into tubules. Although in vivo generation of ER tubules requires direct contact with microtubules, we can rule out an activation

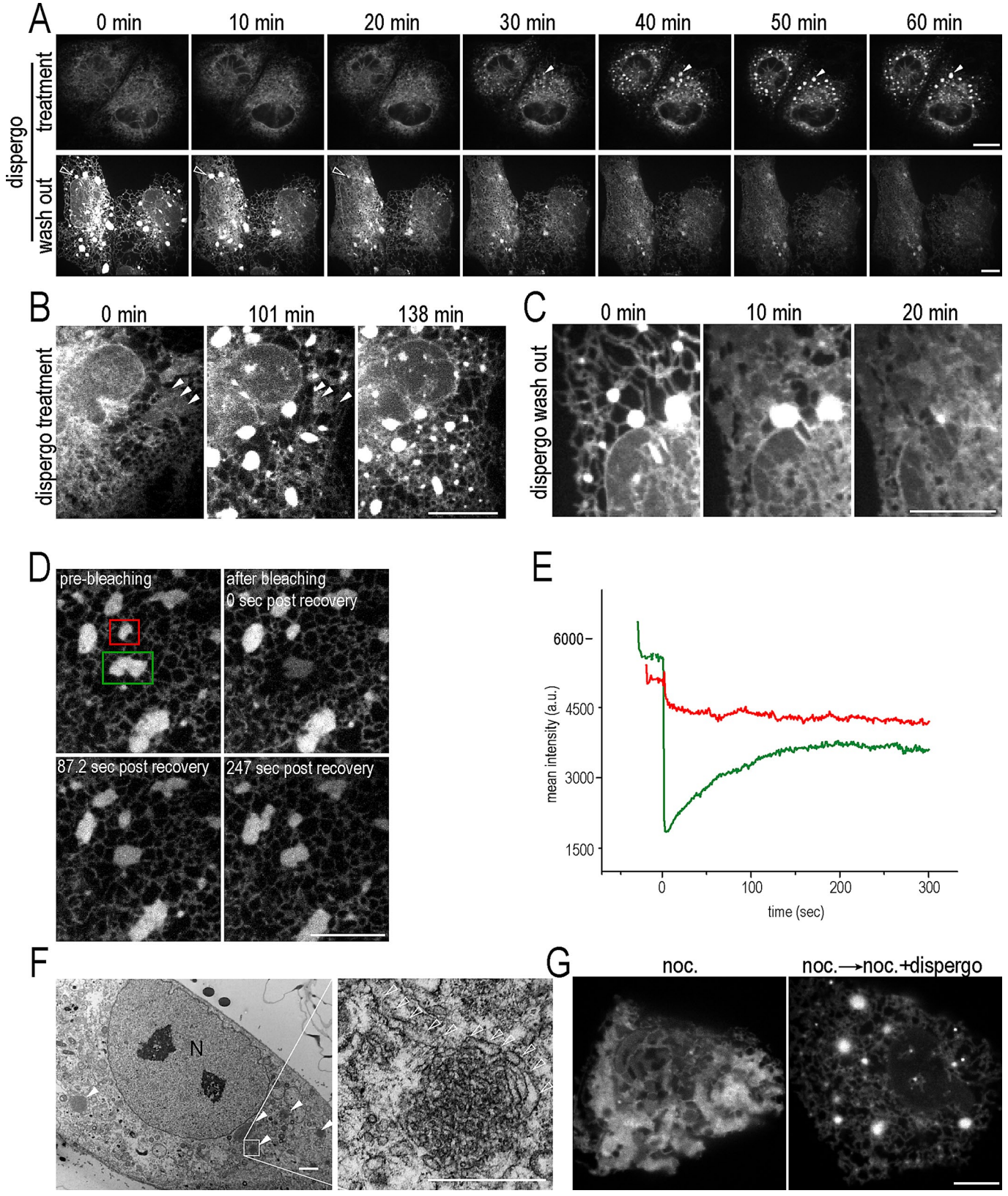

FIGURE 3: Effect of dispergo on the dynamics and morphology of the ER. (A) The effects of dispergo are reversible. Two-dimensional time-lapse series of BSC1 cells stably expressing GFP-Sec61β treated with dispergo for 1 h, showing the gradual appearance of ER patches (top, solid arrowheads; see Supplemental Movie S1). After a further 2-h incubation with dispergo, the compound was removed (bottom). The time-lapse series shows the gradual disappearance of the ER patches (bottom, open arrowheads; see Supplemental Movie S2). (B, C) Two-dimensional time-lapse series from BSC1 cells expressing mRFP1-Sec61β (B) or GFP-Sec61β (C). The images in B highlight the disappearance of ER cisternae (arrowheads) and appearance of ER patches upon dispergo treatment. The images in C are from an enlarged

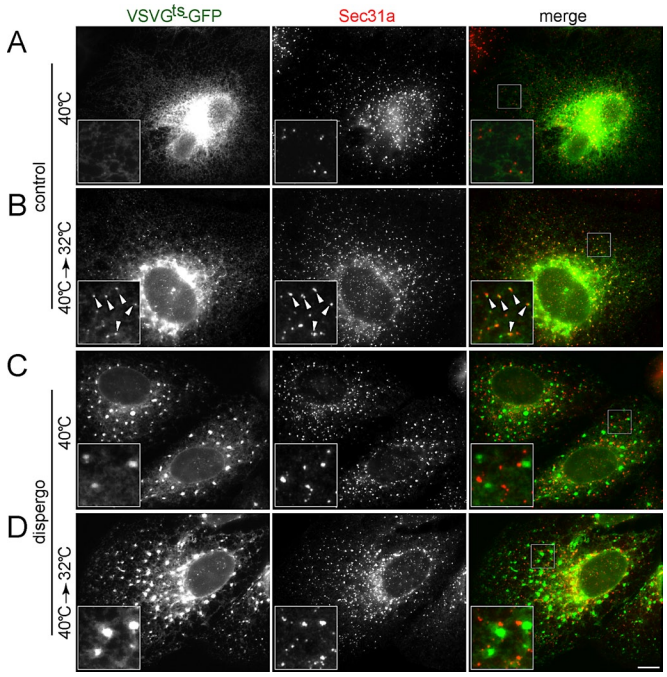

FIGURE 4: Dispergo blocks the recruitment of VSVG^{ts}-GFP to the ERES. BSC1 cells were transduced with adenovirus to express VSVG^{ts}-GFP overnight at 40°C. Cells were treated with either DMSO (control) or dispergo for 40 min (A, C). Subsequently, the temperature was shifted to 32°C for 10 min (40°C→32°C; B, D) before fixation and immunofluorescence detection of endogenous Sec31a. Images were acquired using wide-field fluorescence microscopy. The enlarged boxed regions in the merge images are shown in the bottom left of the corresponding composite images. Arrowheads highlight the colocalization of VSVG^{ts}-GFP with Sec31a in control. Scale bar, 10 μm.

of this interaction since extensive tubulation induced by dispergo is clearly observed in cells lacking microtubules after treatment with nocodazole. Another possibility is that dispergo activates the function of reticulons and DP1/Yop1p family proteins; these molecules localize to regions of high membrane curvature at the edge of the ER cisternae and on ER tubules. Genetic manipulations and in vitro reconstitution studies initially suggested that these proteins drive ER tubulation (Hu *et al.*, 2008), but it has since been proposed that they are instead essential for cisternae formation and stability (Shibata *et al.*, 2010). We do not favor an activator role of dispergo on the function of these proteins, however, since ectopic overexpression of reticulon or DP1/Yop1p proteins did not generate ER patches, prevent export of cargo from the ER, or affect the integrity of the Golgi apparatus (Voeltz *et al.*, 2006; unpublished data). A further possibility is that dispergo inhibits the homotypic fusion of the tubular portion of the ER, leading to the accumulation of ER tubules at the expense of ER cisternae.

The acute ER tubulation induced by dispergo results in the accumulation of ER patches containing a large amount of condensed tubules. This architectural perturbation correlates with a dramatic interference of ER export, to the extent that the contents of the Golgi apparatus are eventually lost, presumably by retention of Golgi constituents in the ER as they traffic constitutively from the Golgi apparatus to the ER. The redistribution of Golgi constituents back to the ER is fundamentally different from that induced by other small molecules such as brefeldin A (Klausner *et al.*, 1992; Supplemental Figure S5D), Exo1 (Feng *et al.*, 2003), or Exo2 (Feng *et al.*, 2004), compounds known to activate a massive tubulation of Golgi membranes and fusion to the ER that correlates with a strong inhibition of ER exit without a detectable change in the organization of the ER. We also do not know why dispergo blocks ER export. One simple explanation is that the extensive ER tubulation induced by dispergo increases membrane tension to such an extent that formation of vesicular carriers is impaired. Protein movement along the dispergo-induced tubules does not seem to be impaired, but certain proteins do accumulate in the tubular ER patches. It is therefore possible that one or more key protein components required for ER exit are mislocalized, thereby impairing the process of carrier formation. Dispergo does not alter the distribution or peripheral density of ERES, although it slightly increases the exchange dynamics of COPII at the ERES sites. Another explanation could be that dispergo affects the lipid homeostasis in the ER, resulting in changes in its shape and function.

The effects of dispergo are reversible, since its removal allows recovery of the ER cisternae at the expense of the densely packed tubular ER patches together with reactivation of ER-to-Golgi traffic, leading to recovery of a functional Golgi with correct morphology. The properties of dispergo and the reversibility of its effects provide new opportunities to study the dynamics and function of the ER. Dispergo will be useful in identifying the molecules and interactions that guide these complex processes.

MATERIALS AND METHODS

Chemical synthesis of dispergo

General procedures. All solid-phase reactions were performed in Poly-Prep Chromatography Columns (Bio-Rad, Hercules, CA) with agitation provided by a Lab-Line 3-D Rotator. After a reaction, the resin was washed in a standard manner: methylene chloride, then tetrahydrofuran, then 2:1 tetrahydrofuran:acetonitrile, and then tetrahydrofuran; this sequence was repeated three times. Methanol was added as needed to dissolve solids. Drying of resin was

region of A, bottom, and show the reversal of these effects upon removal of dispergo. Scale bars, 10 μm. (D) Rapid exchange of GFP-Sec61β within ER patches and with adjacent ER. The images are from a FRAP experiment conducted on an ER patch (green box) in a BSC1 cell stably expressing GFP-Sec61β pretreated with dispergo for 3 h (see Supplemental Movie S3). The ER patch within the unbleached region (red box) was used as a FRAP control. Scale bar, 10 μm. (E) Quantification of the mean fluorescence intensity within the boxed regions of the FRAP experiment. (F) Example of electron microscopy images obtained from BSC1 cells treated with dispergo for 3 h in the absence of ectopic expression of proteins. Left, ER patches highlighted with solid arrowheads. N, nucleus. Scale bar, 2 μm. Right, enlarged highlights of the abundance of relatively circular small membrane profiles contained within the ER patches; membrane profiles ~100 nm in width extending away from the ER patches are highlighted with open arrowheads. Scale bar, 500 nm. (G) Dispergo induces ER tubules and patches in the absence of microtubules. BSC1 cells stably expressing GFP-Sec61β were first treated with nocodazole for 2 h (left), followed by nocodazole and dispergo for an additional 2 h. Scale bar, 10 μm. All fluorescence images were acquired live using spinning disk confocal microscopy.

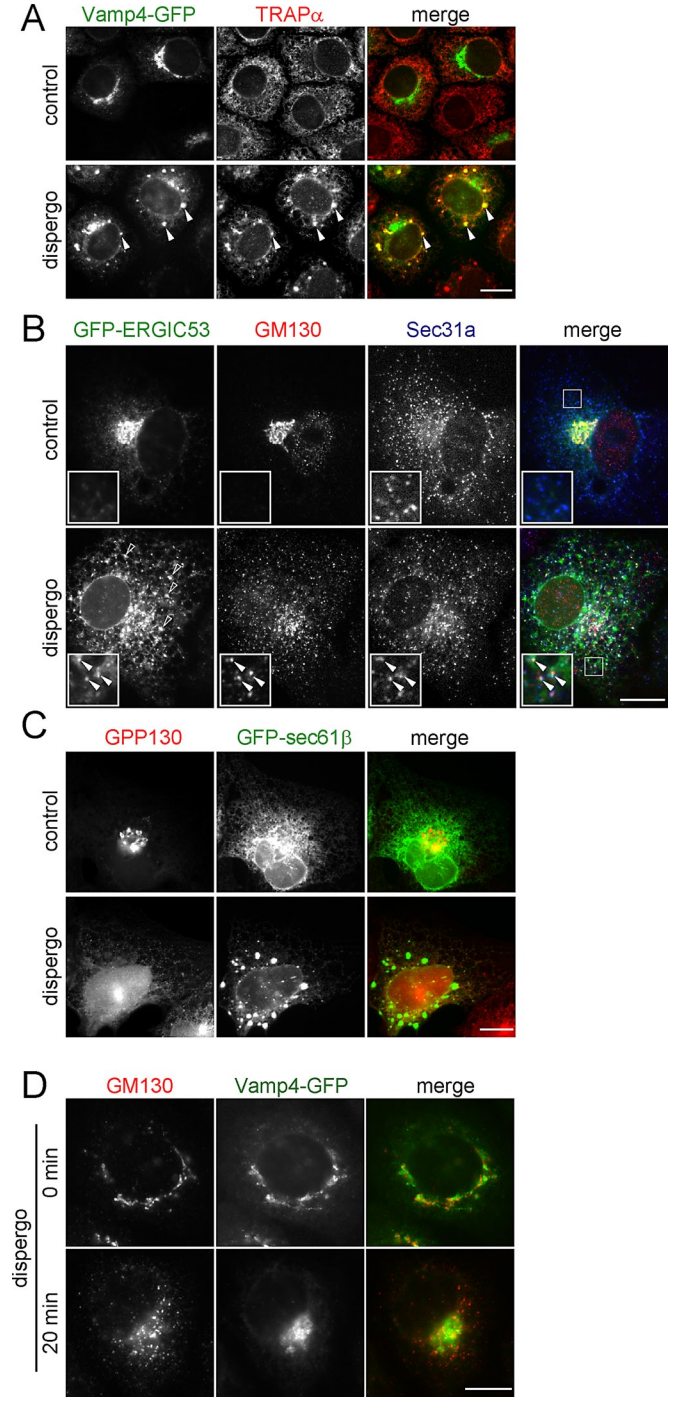

FIGURE 5: Disappearance of the Golgi apparatus and retention of its components in the ER induced by dispergo. (A–C) Cells were treated for 3 h with DMSO (control) or dispergo before immunofluorescence labeling to follow the distributions of several ER (TRAPα, GFP-Sec61β, and Sec31a) and Golgi apparatus (VAMP4-GFP, GM130, ERGIC53-GFP, and GPP130) markers. (A) NRK cells stably expressing Vamp4-GFP immunostained with an anti-TRAPα antibody. Arrowheads highlight the colocalization of Vamp4-GFP and TRAPα in ER patches. (B) BSC1 cells transiently expressing GFP-ERGIC53 immunostained with antibodies specific for GM130 and Sec31a. The arrowheads in the enlarged boxed region highlight colocalization of GFP-ERGIC53 and GM130 at the ERES marked by Sec31a. Empty arrowheads indicate the ERGIC53-positive ER patches induced by dispergo. (C) BSC1 cells stably expressing GFP-Sec61β labeled with anti-GPP130 antibody. The images highlight lack of enrichment of GPP130 in ER patches. (D) Golgi markers had different kinetics of relocation upon dispergo treatment. NRK cells stably expressing Vamp4-GFP without or with dispergo treatment for 20 min were processed for immunofluorescence labeling of GM130. This example highlights that the redistribution of Golgi markers to the ER can occur at different rates (in this case GM130 was faster than Vamp4-GFP). All images were acquired by a wide-field microscope. Scale bars, 10 μm.

performed under house vacuum. Cleavage of resin was performed by swelling the resin in tetrahydrofuran (1 ml per 10 mg of resin), followed by addition of HF-pyridine (200 μl per 10 mg of resin), agitation for 1 h, treatment with methoxytrimethylsilane (1 ml per 10 mg of resin), agitation for 1 h, and filtration. Flash chromatography was performed as described previously (Still et al., 1978) or by using an HPFC Biotage system (Biotage, Uppsala, Sweden) with pre-packed FLASH silica gel columns.

Preparation of dispergo. Cyclopentanethiol (428 μl, 4.0 mmol), 2,6-lutidine (465 μl, 4.0 mmol), and *n*-butyllithium (2.5 M in hexane, 192 μl, 4.0 mmol) were added to a mixture of resin loaded with carpanone-like core (Goess *et al*., 2006), and the resulting mixture was agitated for 24 h. The resin was then subjected to the standard wash and dry procedure outlined in *General procedures*. To the resulting resin was added a premixed solution of *O*-*t*-butylhydroxylamine (804 mg, 6.4 mmol), pyridine (776 μl, 9.6 mmol), and a 1:4 mixture of methanol:methylene chloride (20 ml), and the resulting mixture was agitated for 20 h. The resin was then subjected to the standard wash and dry procedure. To the resulting resin (50 mg, 0.04 mmol) was added tetrahydrofuran (5 ml), followed by HF•pyridine (2 ml), and the resulting mixture was agitated for 2 h. Methoxytrimethylsilane (10 ml) was then added, and the resulting mixture was agitated for 45 min. The mixture was then filtered and washed with methylene chloride, and the combined filtrates were concentrated and the remaining volatiles evaporated under high vacuum. Column chromatography (0:100–4:96 methanol:methylene chloride) afforded 10 mg (54%, three steps) of dispergo. Dispergo was isolated as a 4:1 (*E*/*Z*) mixture of geometrical isomers. ^{1}H nuclear magnetic resonance (NMR; 400 MHz, $CDCl_3$): δ 6.91 (s, 1H), 6.58–6.72 (m, 3H), 6.26–6.36 (m, 1H), 6.13 (bs, 1H), 5.98–6.10 (m, 1H), 5.56–5.64 (m, 1H), 5.36–5.42 (m, 1H), 5.22–5.34 (m, 1H), 4.96–5.04 (m, 1H), 4.86–4.96 (m, 1H), 4.40–4.54 (m, 3H), 3.88–4.12 (m, 3H), 3.76 (bs, 1H), 3.58–3.76 (m, 4H), 3.47 (t, J = 6.0 Hz, 3H), 3.20–3.36 (m, 3H), 2.90–3.04 (m, 2H), 2.65 (dd, J = 14.2, 2.2 Hz, 1H), 2.38 (bs, 1H), 1.05–2.05 (m, 20H), 0.80–1.02 (m, 2H), 0.66–0.80 (m, 2H); ^{13}C NMR (100 MHz, $CDCl_3$): δ 152.81, 152.76, 152.6, 150.3, 145.6, 145.5, 138.1, 134.4, 133.7, 131.6, 127.34, 127.28, 126.9, 122.1, 117.9, 117.6, 116.4, 114.9, 114.8, 113.5, 100.6, 100.2, 78.4, 69.9, 63.1, 62.4, 62.3, 61.7, 61.6, 45.6, 44.3, 42.6, 41.4, 39.8, 39.6, 37.0, 36.7, 35.12, 35.07, 35.0, 34.7, 34.6, 34.4, 34.1, 33.8, 33.5, 33.4, 33.11, 33.06, 32.9, 32.8, 28.0, 27.7, 26.9, 25.1, 24.9, 24.60, 24.57, 24.3, 24.2; IR (neat, cm-1): 3367, 2929, 1624, 1492, 1422, 1196, 1132, 1076; LRMS (ES$^+$): 668 (M^+H^+); HRMS (ES$^+$): calculated for $C_{39}H_{57}NO_6S$, 667.3907; found, 668.3995.

Reagents and antibodies

Nocodazole was from Sigma-Aldrich (St. Louis, MO). Rhodamine–phalloidin and transferrin–Alexa Fluor 488 were from Invitrogen (Carlsbad, CA). Mouse monoclonal antibody against GM130 was from Becton Dickinson (Franklin Lakes, NJ). Rabbit polyclonal antibodies against calreticulin and Giantin were from Abcam (Cambridge, MA). Rabbit polyclonal antibody against β-COP was from EMD Chemicals (San Diego, CA). Hybridoma clone 8g5,

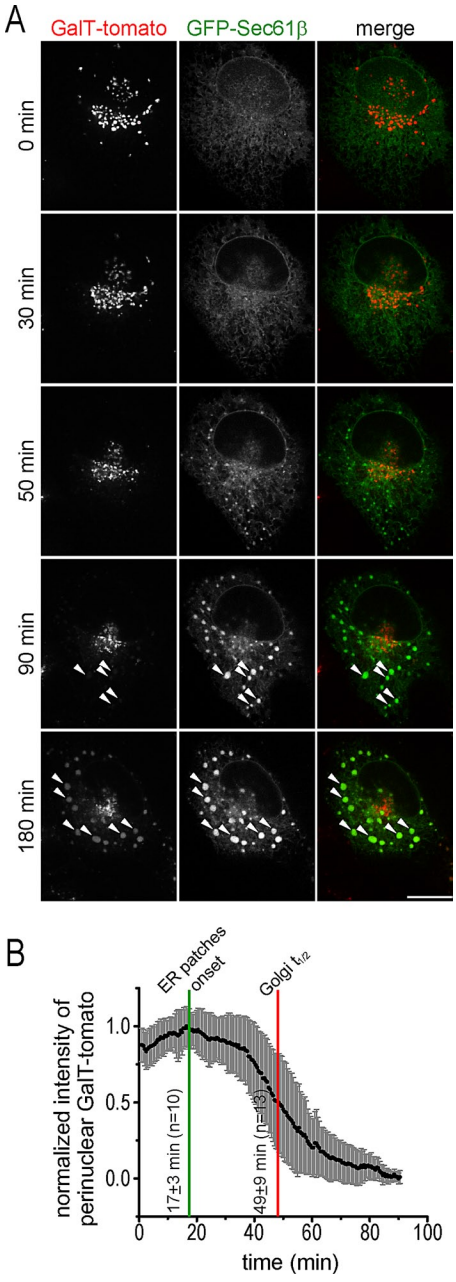

FIGURE 6: Relocalization of the Golgi marker GalT-tomato to the ER induced by dispergo. (A) BSC1 cell transiently expressing GalT-tomato and GFP-Sec61β were treated with dispergo and imaged by spinning disk confocal microscopy (see Supplemental Movie S4). Arrowheads highlight colocalization of GalT-tomato and GFP-Sec61β at ER patches marked by GFP-Sec61β. Scale bar, 10 μm. (B) Time dependence for the loss of GalT-tomato from the perinuclear region corresponding to the Golgi apparatus induced by dispergo in BSC1 cells stably expressing GalT-tomato. The fluorescence intensity of GalT-tomato at the perinuclear region determined before dispergo addition was used to normalize the data. Plot shows mean values and SD for each time point ($n = 13$ cells). Golgi $t_{1/2}$ represents the mean time ± SD that it took for the signal of GalT-tomato to be reduced by 50%. "ER patches onset" marks the time at which the appearance of ER patches labeled with GFP-Sec61β was first detected ($n = 10$ cells).

which secretes mouse monoclonal antibody against VSVG extracellular domain, was obtained from the American Type Culture Collection (Rockville, MD). Mouse monoclonal antibodies against CD63 and Lamp1 were obtained from the Developmental Studies Hybridoma Bank (University of Iowa, Iowa City, IA). Rabbit polyclonal antibodies against Sec31a and Golgin97 were from W. Hong (Institute of Molecular and Cell Biology, Singapore). Rabbit polyclonal antibody against TRAPα was from T. Rapaport (Harvard Medical School, Boston, MA). Rabbit polyclonal and mouse monoclonal antibodies against GPP130 were from A. Linstedt (Carnegie Mellon University, Pittsburgh, PA). Goat anti-mouse and rabbit secondary antibodies conjugated with either Alexa Fluor 488 or 594 were purchased from Invitrogen.

DNA plasmids

To clone GalT-tomato, an insert containing the coding sequence of amino acids 1–81 of β-galactosyltransferase (GalT) was released by digesting pEYFP-Golgi plasmid (Takara Bio, Shiga, Japan) using *Nhe*I/*Bam*HI and subsequently ligated into *Nhe*I/*Bam*HI-digested ptdTomato-N1 vector (Takara Bio) to make plasmid GalT-tomato. Plasmids Sec61β in pAcGFP1-C1 (Takara Bio), HA-DP1 in pcDNA3, and Sec61β-mRFP1 were from T. Rapaport. Plasmid ERGIC53-GFP was from H.-P. Hauri (University of Basel, Basel. Switzerland). Plasmid expressing GFP–α-tubulin was from Takara Bio.

Cell culture, transfection, and stable cell lines

BSC1 and HeLa cells were obtained from the American Tissue Culture Collection. Cells were cultured at 37°C in DMEM supplemented with 10% fetal bovine serum. The transfection experiments were performed using FuGENE 6 transfection reagent (Roche, Basel, Switzerland) according to the manual.

To generate cell lines stably expressing GalT-tomato or GFP-Sec61β, BSC1 cells were transfected with either GalT-tomato or GFP-Sec61β. Pooled stable cells were selected in medium containing 0.5 mg/ml G418 (Invitrogen) and subsequently replated at very low density to obtain single colonies of cells. Colonies were screened by fluorescence microscopy, isolated, and subsequently expanded. NRK (normal rat kidney) cells stably expressing Vamp4-GFP (Tran *et al.*, 2007) were from W. Hong. All stable cell lines were maintained in medium supplemented with 0.1 mg/ml G418.

Dispergo, nocodazole, brefeldin A, tunicamycin, and DTT treatments

Dispergo was dissolved in dimethyl sulfoxide (DMSO) to make a 10 mM stock solution and stored at –20°C. The stock solution was directly diluted in culture medium to a final working concentration of 20 μM. DMSO, 0.2%, was used as control in parallel with dispergo treatments. Nocodazole was dissolved in DMSO at a concentration of 33 mM and stored at –20°C. The final working concentration of nocodazole was 16.5 μM dissolved in culture medium. Brefeldin A and tunicamycin were also dissolved in DMSO as 10 mM stock solutions, which were then directly diluted in culture medium to a final working concentration of 10 μM. DTT was dissolved in water to make a 100 mM stock, and the final working concentration of 100 μM was achieved by directly diluting the stock in culture medium.

Immunostaining

Cells grown on round glass coverslips were fixed in 4% paraformaldehyde in phosphate-buffered saline (PBS) for 20 min at room temperature. Paraformaldehyde was subsequently blocked by incubation with 100 mM NH_4Cl. After extensive washes with PBS, cells were simultaneously permeabilized and stained with the required antibodies diluted in PBS containing 0.1% saponin, 5% fetal bovine serum, and 2% bovine serum albumin. Coverslips were mounted in Mowiol and sealed with nail polish.

VSVG^{ts}-GFP trafficking assays

Recombinant adenovirus expressing a temperature-sensitive mutant vesicular stomatitis virus glycoprotein G (VSVGts) fused to GFP (VSVG^{ts}-GFP) was generated by subcloning the PCR fragment spanning cytomegalovirus promoter-VSVG^{ts}-GFP-poly(A) into the *Not*I site of the pShuttle vector, followed by viral packaging as described previously (He *et al*., 1998). BSC1 cells plated on glass coverslips were infected with the adenovirus overnight in a 40°C CO_2 incubator. Cells were subsequently incubated with media containing dispergo at 40°C for 40 or 60 min and transferred to 32°C to release VSVG^{ts}-GFP for various lengths of time as indicated before immunofluorescence microscopy.

Fluorescence microscopy

Wide-field epifluorescence microscopy of fixed samples was performed on an upright microscope (Axioskop; Carl Zeiss, Thornwood, NY), equipped with a 63×/numerical aperture 1.4 Plan-Apochromatic oil immersion objective lens, a motorized focus unit (Applied Scientific Instrumentation, Eugene, OR), a spherical aberration correction device (Infinity Photo-Optical, Boulder, CO), and a cooled charge-coupled device (CCD) camera (Roper CoolSnap HQ; Photometrics, Tucson, AZ). Spinning disk confocal fluorescence images were acquired with an inverted microscope, Axiovert 200M (Carl Zeiss), equipped with a spinning disk confocal head (CSU10 or 22; Yokogawa Electric, Tokyo, Japan), a spherical aberration correction device (Infinity Photo-Optical), an electron-multiplying CCD camera (Cascade 512B; Photometrics), and 473- and 561-nm laser light sources (Crystal Lasers, Reno, NV). The two-dimensional time-lapse imaging described in Figure 6B was conducted in an inverted wide-field microscope, Axiovert 200M, equipped with a cooled CCD camera (Roper CoolSnap HQ). Microscopes were controlled under SlideBook software (Intelligent Imaging Innovations, Denver, CO). Live-cell imaging was performed as previously described (Lu *et al*., 2009, 2011). To quantify the perinuclear intensity of GalT-tomato described in Figure 6B, time-lapse images were subjected to segmentation, and the total intensity of the masked perinuclear region of each cell was summed at each time point. Series of intensity values as a function of elapsed time were normalized and plotted using OriginPro 8 (Origin Lab, Northampton, MA).

Electron microscopy

Samples were chemically fixed using 2.5% glutaraldehyde in 0.1 M cacodylate buffer for 1 h, postfixed with 1% osmium tetroxide, followed by 1% uranyl acetate and then dehydrated with serial dilutions of ethanol. Samples were embedded in resin, cut into thin sections, stained with uranyl acetate followed by lead acetate, and viewed on a 1200EX transmission electron microscope at 80 kV (JEOL, Peabody, MA).

ACKNOWLEDGMENTS

We thank M. Ericsson for help with electron microscopy and E. Marino for maintaining the imaging resources in the Kirchhausen laboratory, and Yoshiki Tanaka for assistance with the nuclear magnetic resonance, infrared, and high-resolution mass spectrometry characterization of dispergo. R.H. was a recipient of postdoctoral fellowships from the Canadian Institutes of Health Research and National Sciences and Engineering Research Council of Canada. B.G. was a recipient of a doctoral fellowship from the U.S. Department of Defense (National Defense Science and Engineering Graduate Fellowship). This work was supported in part by National Institutes of Health Grant GM-075252 (to T.K.) and U54 AI057159 (New England Regional Center of Excellence in Biodefense and Emerging Infectious Disease, Core Imaging Facility, Boston, MA), as well as P01 GM62556 (to T.K. and M.S.) and SBS SUG M58080013 (to L.L.).

REFERENCES

Baumann O, Walz B (2001). Endoplasmic reticulum of animal cells and its organization into structural and functional domains. Int Rev Cytol 205, 149–214.

de Brito OM, Scorrano L (2010). An intimate liaison: spatial organization of the endoplasmic reticulum-mitochondria relationship. EMBO J 29, 2715–2723.

Emr S *et al*. (2009). Journeys through the Golgi—taking stock in a new era. J Cell Biol 187, 449–453.

Feng Y, Jadhav AP, Rodighiero C, Fujinaga Y, Kirchhausen T, Lencer WI (2004). Retrograde transport of cholera toxin from the plasma membrane to the endoplasmic reticulum requires the *trans*-Golgi network but not the Golgi apparatus in Exo2-treated cells. EMBO Rep 5, 596–601.

Feng Y, Yu S, Lasell TK, Jadhav AP, Macia E, Chardin P, Melancon P, Roth M, Mitchison T, Kirchhausen T (2003). Exo1: a new chemical inhibitor of the exocytic pathway. Proc Natl Acad Sci USA 100, 6469–6474.

Forster R, Weiss M, Zimmermann T, Reynaud EG, Verissimo F, Stephens DJ, Pepperkok R (2006). Secretory cargo regulates the turnover of COPII subunits at single ER exit sites. Curr Biol 16, 173–179.

Friedman JR, Lackner LL, West M, DiBenedetto JR, Nunnari J, Voeltz GK (2011). ER tubules mark sites of mitochondrial division. Science 334, 358–362.

Goess BC, Hannoush RN, Chan LK, Kirchhausen T, Shair MD (2006). Synthesis of a 10,000-membered library of molecules resembling carpanone and discovery of vesicular traffic inhibitors. J Am Chem Soc 128, 5391–5403.

He TC, Zhou S, da Costa LT, Yu J, Kinzler KW, Vogelstein B (1998). A simplified system for generating recombinant adenoviruses. Proc Natl Acad Sci USA 95, 2509–2514.

Hu J, Shibata Y, Voss C, Shemesh T, Li Z, Coughlin M, Kozlov MM, Rapoport TA, Prinz WA (2008). Membrane proteins of the endoplasmic reticulum induce high-curvature tubules. Science 319, 1247–1250.

Klausner RD, Donaldson JG, Lippincott-Schwartz J (1992). Brefeldin A: insights into the control of membrane traffic and organelle structure. J Cell Biol 116, 1071–1080.

Kreykenbohm V, Wenzel D, Antonin W, Atlachkine V, von Mollard GF (2002). The SNAREs vti1a and vti1b have distinct localization and SNARE complex partners. Eur J Cell Biol 81, 273–280.

Lee MC, Miller EA, Goldberg J, Orci L, Schekman R (2004). Bi-directional protein transport between the ER and Golgi. Annu Rev Cell Dev Biol 20, 87–123.

Linstedt AD, Foguet M, Renz M, Seelig HP, Glick BS, Hauri HP (1995). A C-terminally-anchored Golgi protein is inserted into the endoplasmic reticulum and then transported to the Golgi apparatus. Proc Natl Acad Sci USA 92, 5102–5105.

Linstedt AD, Mehta A, Suhan J, Reggio H, Hauri HP (1997). Sequence and overexpression of GPP130/GIMPc: evidence for saturable pH-sensitive targeting of a type II early Golgi membrane protein. Mol Biol Cell 8, 1073–1087.

Lu L, Ladinsky MS, Kirchhausen T (2009). Cisternal organization of the endoplasmic reticulum during mitosis. Mol Biol Cell 20, 3471–3480.

Lu L, Ladinsky MS, Kirchhausen T (2011). Formation of the postmitotic nuclear envelope from extended ER cisternae precedes nuclear pore assembly. J Cell Biol 194, 425–440.

Lu L, Tai G, Hong W (2004). Autoantigen Golgin-97, an effector of Arl1 GTPase, participates in traffic from the endosome to the *trans*-Golgi network. Mol Biol Cell 15, 4426–4443.

Luzio JP, Brake B, Banting G, Howell KE, Braghetta P, Stanley K (1990). Identification, sequencing and expression of an integral membrane protein of the *trans*-Golgi network (TGN38). Biochem J 270, 97–102.

Nakamura N, Rabouille C, Watson R, Nilsson T, Hui N, Slusarewicz P, Kreis TE, Warren G (1995). Characterization of a *cis*-Golgi matrix protein, GM130. J Cell Biol 131, 1715–1726.

Oprins A, Duden R, Kreis TE, Geuze HJ, Slot JW (1993). Beta-COP localizes mainly to the cis-Golgi side in exocrine pancreas. J Cell Biol 121, 49–59.

Pelish HE *et al*. (2006). Secramine inhibits Cdc42-dependent functions in cells and Cdc42 activation in vitro. Nat Chem Biol 2, 39–46.

Schindler R, Itin C, Zerial M, Lottspeich F, Hauri HP (1993). ERGIC-53, a membrane protein of the ER-Golgi intermediate compartment, carries an ER retention motif. Eur J Cell Biol 61, 1–9.
Shibata Y, Shemesh T, Prinz WA, Palazzo AF, Kozlov MM, Rapoport TA (2010). Mechanisms determining the morphology of the peripheral ER. Cell 143, 774–788.
Shibata Y, Voeltz GK, Rapoport TA (2006). Rough sheets and smooth tubules. Cell 126, 435–439.
Snapp EL, Hegde RS, Francolini M, Lombardo F, Colombo S, Pedrazzini E, Borgese N, Lippincott-Schwartz J (2003). Formation of stacked ER cisternae by low affinity protein interactions. J Cell Biol 163, 257–269.
Sprocati T, Ronchi P, Raimondi A, Francolini M, Borgese N (2006). Dynamic and reversible restructuring of the ER induced by PDMP in cultured cells. J Cell Sci 119, 3249–3260.
Steegmaier M, Klumperman J, Foletti DL, Yoo JS, Scheller RH (1999). Vesicle-associated membrane protein 4 is implicated in *trans*-Golgi network vesicle trafficking. Mol Biol Cell 10, 1957–1972.
Still C, Kahn M, Mitra A (1978). Rapid chromatographic technique for preparative separations with moderate resolution. J Org Chem 43, 2923–2925.
Storrie B (2005). Maintenance of Golgi apparatus structure in the face of continuous protein recycling to the endoplasmic reticulum: making ends meet. Int Rev Cytol 244, 69–94.
Tang BL, Wong SH, Qi XL, Low SH, Hong W (1993). Molecular cloning, characterization, subcellular localization and dynamics of p23, the mammalian KDEL receptor. J Cell Biol 120, 325–338.
Terasaki M, Chen LB, Fujiwara K (1986). Microtubules and the endoplasmic reticulum are highly interdependent structures. J Cell Biol 103, 1557–1568.
Tran T, Zeng Q, Hong W (2007). VAMP4 cycles from the cell surface to the trans-Golgi network via sorting and recycling endosomes. J Cell Sci 120, 1028–1041.
Varadarajan S *et al*. (2012). A novel cellular stress response characterised by a rapid reorganisation of membranes of the endoplasmic reticulum. Cell Death Differ 19, 1896–1907.
Voeltz GK, Prinz WA, Shibata Y, Rist JM, Rapoport TA (2006). A class of membrane proteins shaping the tubular endoplasmic reticulum. Cell 124, 573–586.
Waterman-Storer CM, Salmon ED (1998). Endoplasmic reticulum membrane tubules are distributed by microtubules in living cells using three distinct mechanisms. Curr Biol 8, 798–806.